# Optical Coherence Tomography of Tumor Spheroids Identifies Candidates for Drug Repurposing in Ovarian Cancer

Feng Yan<sup>†</sup>, Ji-Hee Ha<sup>†</sup>, Yuyang Yan, Sam B. Ton, Chen Wang, Bornface Mutembei, Zaid A. Alhajeri, Aubrey F. McNiel, Andrew J. Keddissi, Qinghao Zhang, Muralidharan Jayaraman, Danny N. Dhanasekaran\* and Qinggong Tang\*

Abstract— Objective: Multicellular tumor spheroids (MCTs) are indispensable models for evaluating drug efficacy for precision cancer therapeutic strategies as well as for repurposing FDAapproved drugs for ovarian cancer. However, current imaging techniques cannot provide effective monitoring of pathological responses due to shallow penetration and experimentally operative destruction. We plan to utilize a noninvasive optical imaging tool to achieve in vivo longitudinal monitoring of the growth of MCTs and therapeutic responses to repurpose three FDA-approved drugs for ovarian cancer therapy. Methods: A swept-source optical coherence tomography (SS-OCT) system was used to monitor the volume growth of MCTs over 11 days. Three inhibitors of 2-Methoxyestradiol (2-ME), AZD1208, and R-Ketorolac (R-keto) with concentrations of 1, 10, and 25 µM were employed to treat ovarian MCTs on day 5. Three-dimensional (3D), intrinsic optical attenuation contrast, and degree of uniformity were applied to analyze the therapeutic effect of these inhibitors on ovarian MCTs. Results: We found that 2-ME, AZD1208, and R-keto with concentration of 10 and 25 µM significantly inhibited the volume growth of ovarian MCTs. There was no effect to necrotic tissues from all concentrations of 2-ME, AZD1208, and R-keto inhibitors from our OCT results. 2-ME and AZD1208 inhibited the growth of high uniformity tissues within MCTs and higher concentrations provided more significant inhibitory effects. Conclusion: Our results indicated that OCT was capable and reliable to monitor the therapeutic effect of inhibitors to ovarian MCTs and it can be used for the rapid characterization of novel therapeutics for ovarian cancers in the future.

Index Terms— Optical coherence tomography, Multicellular tumor spheroid, Ovarian cancer, 2-Methoxyestradiol, AZD1208, R-ketorolac

This work was supported by grants from the University of Oklahoma Health Sciences Center (3P30CA225520), Faculty Investment Program from University of Oklahoma, Institutional Research Grant number IRG-19-142-01 from the American Cancer Society, National Science Foundation (OIA-2132161), National Institute of Health (R01DK133717), the medical imaging COBRE (P20 GM135009). Histology service provided by the Tissue Pathology Shared Resource was supported in part by the National Institute of General Medical Sciences COBRE Grant P20GM103639 and National Cancer Institute Grant P30CA225520 of the National Institutes of Health.

Feng Yan, Yuyang Yan, Sam B. Ton, Chen Wang, Bornface Mutembei, Zaid A. Alhajeri, Aubrey F. McNiel, Andy J. Keddissi, Qinghao Zhang are with the

#### I. INTRODUCTION

EPITHELIAL ovarian cancer is the most lethal gynecologic cancer, largely due to the preponderance of the advanced stage disease upon diagnosis and the high rates of recurrence and development of resistance to the conventional chemotherapy. Although improvements in the front-line treatment options have resulted in an 80% rate of remission, unfortunately, fewer than 50% of patients remain alive at 5 years [1]. Given the poor overall survival rate for women diagnosed with epithelial ovarian cancer and the considerable toxicities that patients encounter with the conventional chemotherapies, identification and development of the novel agents and targeted therapeutic methods are critically needed to improve the efficacy of epithelial ovarian cancer treatment and enhance the overall clinical outcomes of the patients. In order to more effectively treat cancer patients in oncology, repurposing of FDA-approved drugs is an increasingly popular strategy due to the financial and logistical constraints of new drug development. For rapid screening of drug repurposing, three-dimensional (3D) multicellular tumor spheroids (MCTs) have proved to be an advanced tumor model. It has been increasingly realized that MCTs provides an experimental intermediary between in vitro and in vivo models, in addition to its greater resemblance with the in vivo solid tumor physiology [2]. The cells within the MCTs interact with each other closely and they mimic the in vivo tumor cells that exist within the tumor microenvironment in properties such as growth, metabolism, and therapeutic resistance [3-6]. Thus, it serves as an ideal experimental model for studies involving cancer research and anti-cancer drug screening.

In spite of these advantages of using MCTs for numerous

Stephenson School of Biomedical Engineering, University of Oklahoma, Norman, OK 73019, USA. Ji-Hee Ha, Muralidharan Jayaraman and \*Danny N. Dhanasekaran are with Department of Cell Biology, The University of Oklahoma Health Sciences Center, Oklahoma City, OK 73104, USA (correspondence e-mail: <a href="mailto:danny-dhanasekaran@ouhsc.edu">danny-dhanasekaran@ouhsc.edu</a>). \*Qinggong Tang is with the Stephenson School of Biomedical Engineering, University of Oklahoma, Norman, OK 73019, USA and with the Institute for Biomedical Engineering, Science, and Technology (IBEST), University of Oklahoma, Norman, OK 73019, USA. (correspondence e-mail: <a href="mailto:qtang@ou.edu">qtang@ou.edu</a>). †Feng Yan and †Ji-Hee Ha have equal contributions.

cancer studies, the currently available methods to monitor and analyze the 3D structure of MCTs face several limitations, e.g., the destruction of the MCTs morphology during analysis owing to extreme conditions in the procedures and the technical limitations in the imaging penetration depth with the MCTs analysis [7, 8]. Moreover, the invasive and dye-based observation modalities restrict the *in vivo* longitudinal tracking of MCTs morphology and physiology. This necessitates the need for a better tool for MCTs analysis that can aid studies on drug screening as well as other cancer research employing the MCTs.

Optical coherence tomography (OCT) is a non-invasive and label-free imaging modality that can achieve micrometermagnitude resolution images within biological materials [9]. Because of the advantage of providing non-destructive spatial and depth-resolved information, OCT has been used to achieve in vitro imaging of MCTs growth and detect the in vivo necrotic tissue progression based on the intrinsic optical attenuation contrast [7, 8, 10]. Moreover, OCT has been used to observe anti-cancer drug responses by monitoring the spheroid morphology, growth, and cell death [10-13]. Particularly, OCT has been used to measure the change of spheroid volume growth [12] and the metabolic activity of the necrotic process [10] within MCTs for monitoring the drug response up to 48 hours. However, the use of OCT imaging techniques to measure internal structural change of spheroids as well as drug diffusion and therapeutical pathways of different anti-cancer inhibitors within MCTs over a relatively longer monitoring time has not been reported, and the effectiveness remains unknown.

In this study, to evaluate the repurposing potential of three different FDA-approved drugs for ovarian cancer therapy, a swept-source optical coherence tomography (SS-OCT) imaging platform was used to obtain longitudinal twodimensional (2D) and 3D structures of the ovarian MCTs, noninvasively, over a span of 11 days, in situ. The growth mode, necrosis progression, and uniformity distribution of tumor cells within ovarian MCTs were analyzed in OCT intensity images to observe the microenvironment change of MCTs. This study characterized the inhibitory effects of three different FDAapproved drugs, namely R-Ketorolac (R-keto), a Rac1/CDC42 inhibitor [14], 2-Methoxystradiol (2-ME), a HIF-1α inhibitor [15], and AZD1208, a pan-Pim kinase inhibitor [16] on ovarian MCTs' growth and identified the most effective inhibitor that interfered with the growth of these ovarian MCTs using the SS-OCT imaging platform. In addition, histological staining of the MCTs using H&E staining as well as MCTs imaging using Operetta were also carried out for a comparative analysis.

#### II. METHODS AND MATERIALS

### A. Cell Culture

High grade serous carcinoma cell line OVCAR4 was maintained in Roswell Park Memorial Institute (RPMI) 1640 medium (Cellgro, Manassas, VA), at 37°C in a 5% CO2 incubator. The medium was supplemented with 10% FBS (Gemini Bio-Products, West Sacramento, CA), 50 U/mL penicillin and 50 μg/mL streptomycin (Cellgro, Manassas,

VA).

#### B. Spheroid Formation and Inhibitor Treatment

OVCAR4 cells were seeded at a density of 5,000 cells/well in a 96-well non-adherent round bottom cell culture plates (CellCarrier  $^{TM}$ -96 spheroid ULA plates) at day 0, as shown in Fig. S1. From the following day (day 1), cells were imaged every day until  $11^{th}$  day, by swept-source optical coherence tomography (SS-OCT) imaging system, on both 2D and 3D modes. On the  $5^{th}$  day, the inhibitors namely R-keto, 2-ME, and AZD1208, and 0.05% Dimethyl Sulfoxide (DMSO) as control group were added individually into each well at concentration of 1, 10, and 25  $\mu M$  respectively, resulting in 10 groups with 12 MCTs (wells) per group. On the  $11^{th}$  day, the cells were collected for histology staining as well as spheroid imaging with Operetta.

## C. Swept-Source Optical Coherence Tomography Imaging System

A swept-source optical coherence tomography (SS-OCT) system reported in our previous study [8], was used to perform the 2D and 3D imaging for MCTs. A central wavelength of 1300 nm and a scanning frequency of 200 kHz laser were utilized in this system to provide an axial resolution of 14  $\mu m$  and a lateral resolution of 20  $\mu m$  in air. This system provided a maximum imaging depth of 8.0 mm in air and a sensitivity of 98 dB at the 200 kHz. A commercialized objective (OCT-LK3, Thorlabs, New Jersey) with the focal length of 36 mm in this system was employed to achieve a maximum field of view (FOV) of 10 mm  $\times$  10 mm.

#### D. Scanning Protocol and Measurement

To achieve the longitudinal imaging of MCTs under a sterile environment and avoiding the bacterial infections, a custom-made motion stage for SS-OCT scanner was built to put the scanner into the biosafety cabinet for imaging. In the 11 days measurement, every spheroid within the plate well was imaged in the biosafety cabinet. A 3 mm  $\times$  3 mm FOV was used to cover the entire region based on the center of the well for each imaging. The pixel number in the FOV in this protocol was 600  $\times$  600 to provide a sampling resolution of 5  $\mu m \times$  5  $\mu m$ . The total imaging time for each spheroid was  $\sim$ 3.0 seconds.

#### E. Histological Staining of Spheroids

On the 11<sup>th</sup> day, one set of the plates was used for histological staining. Briefly, the growth media was removed, and washed with PBS. The spheroids were fixed with 4% paraformaldehyde solution for 15 minutes and moved into 70% ethanol. The 70% ethanol was removed and Histogel<sup>TM</sup> (ThermoFisher) was added to encapsulate the spheroids, following the manufacturer's protocol. The spheroids in Histogel<sup>TM</sup>, were processed for embedding in paraffin blocks. Subsequently, 4-micron thickness sections from the blocks were cut for staining. Hematoxylin and Eosin (H&E) staining was carried out using a

Leica Multistainer and sealed with the coverslips. The H&E stained sections were imaged at 10X magnification on a Nikon upright microscope.

#### F. Spheroids imaging using Operetta

On the 5<sup>th</sup> day of the spheroid culture, 25 nM of Incucyte<sup>®</sup> Cytotox Red dye was added to each well before the addition of the inhibitors to detect the dead cells. On the 11th day, the plates were imaged using brightfield and far-red (excitation at 612 nm and emission at 632 nm) with Perkin Elmer Operetta<sup>TM</sup>, high content high throughput imaging system. The red fluorescence intensity was used to evaluate the number of dead cells, post-inhibitor treatment. A magnification of 2X was used to capture the spheroidal images using Operetta<sup>TM</sup>.

#### G. Image processing and calculating

Necrotic tissue detection. The intrinsic optical attenuation

coefficient based on the degree of the intensity attenuation along the axial direction in OCT structural images was used to detect necrotic tissues within MCTs. The average value between the two peaks of the probability distribution of the attenuation coefficient from 12 spheroids on day 10 in the control group was employed to distinguish the normal and necrotic tissues within MCTs. The detailed calculation of attenuation coefficient had been described in our previous work [8]. Briefly, the intensity profile within tumor spheroids showed two distinct slopes. The slow decay of intensity signal indicates active proliferation cells, and the fast decay indicates denser dead cells. The high and low attenuation regions were able to indicate normal and necrotic regions within MCTs, respectively.

Tissue uniformity distribution. Based on the intensity distribution of OCT structural images, the standard deviation of the difference between each pixel value and surrounding 4-pixel values in 4 directions (0°, 45°, 90°, 135°) was utilized to

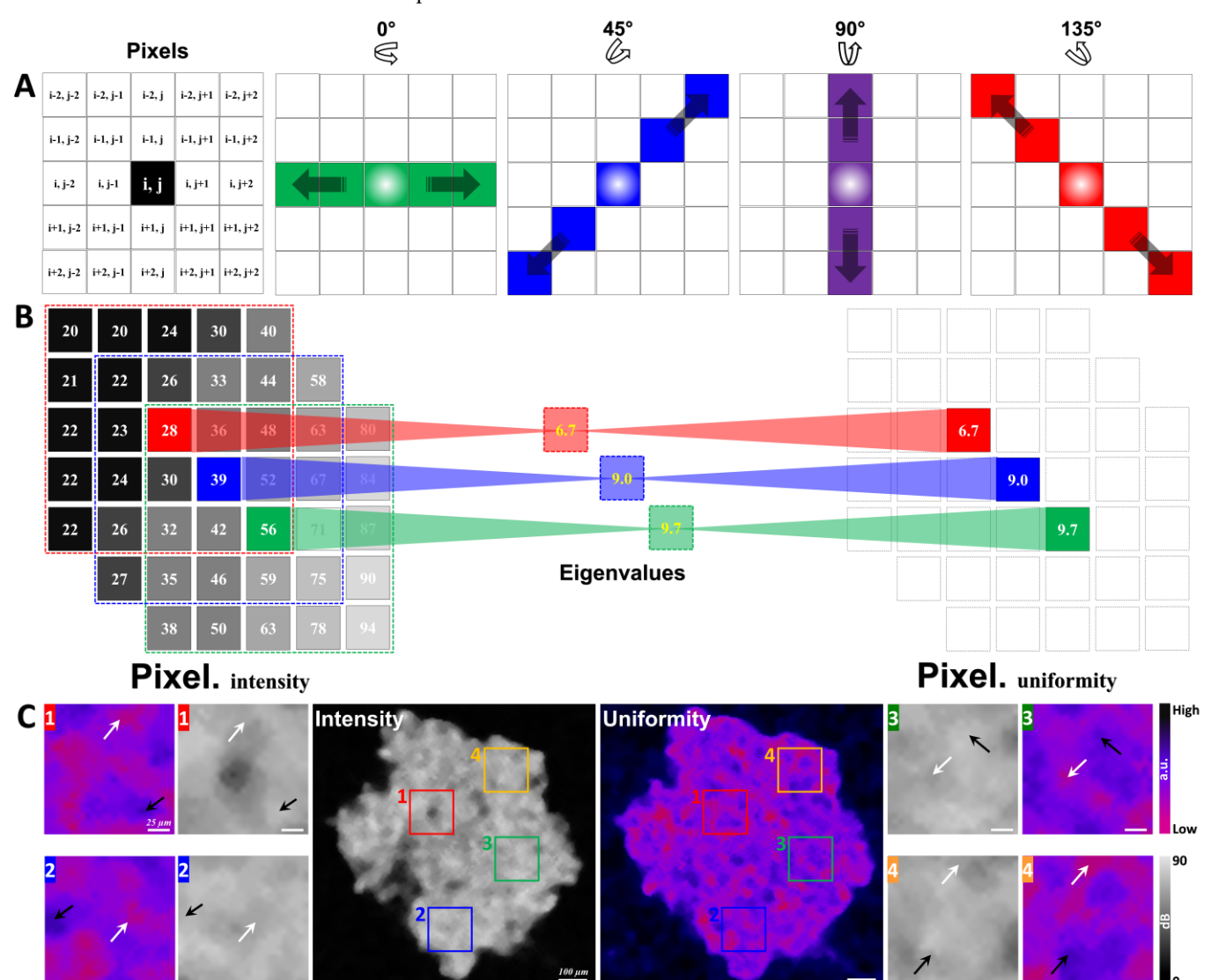


Fig. 1. The flow chart of the uniformity calculation and the comparison between OCT intensity and uniformity distribution. A, the concept of uniformity calculation. B, the transfer calculation of OCT intensity and uniformity. C, representative images of OCT intensity and uniformity distribution. Black and white arrows in C1-4 indicate relatively homogeneous and heterogeneous areas, respectively; black and white arrows indicate the corresponding high- and low-uniformity areas in the calculated uniformity images.

assess the uniform degree of tissues within MCTs, as shown in Fig. 1A. Fig. 1B showed the calculation process from pixel intensity matrix to uniformity coefficient matrix. The uniform degree indicated the dispersion degree of intensity difference in a specific area to reveal the distribution characterization of cell densities. Lower values (~0) represented more homogeneous tissue distribution and higher values (~1) represented more heterogeneous tissue distribution in MCTs. Fig. 1C showed the representative images of OCT intensity and uniformity distribution on day 5. With four enlarged specific regions from intensity and uniformity images, we observed the trend of uniformity distribution of cells within MCTs that were not observed directly from OCT intensity images. The areas with relatively homogeneous (black arrows) and heterogeneous (white arrows) intensity values in OCT images have been transferred to high-uniform (black arrows) and low-uniform (white arrows) degree regions, respectively, in a higher contrast mode (Fig. 1C). The distribution characterization of tissue uniformity based on the OCT intensity could be used to monitor the change of cell growth and proliferation within MCTs.

#### H. Statistical analyses

To compare the difference among the volume growth, necrotic tissue formation, and uniformity distribution within in MCTs, the paired student t-test was performed as each time point in different inhibitors. A P-value of < 0.05 was utilized to indicate the statistics between the paired measurements was significant.

#### III. RESULTS

#### A. Tumor spheroid growth dynamics

SS-OCT was used to perform 2D and 3D imaging of OVCAR4 tumor spheroids with inhibitors of 2-ME, AZD1208, and R-keto with concentrations of 1, 10, and 25  $\mu M$  over 11 days. Fig. 2 showed the volume growth of OVCAR4 MCTs at different conditions for 11 days. Enface (XY), cross-sectional (XZ in depth direction), and 3D (color) rendered images were shown to illustrate the growth dynamics of corresponding samples. We observed that OVCAR MCTs formed irregular spheroids on day 1. The height and enface area of the spheroids increased over 11 days. With inhibitors, 2-ME at 10 and 25  $\mu M$  and AZD1208 at 25  $\mu M$ , the MCTs showed lower spheroid heights compared to control samples.

To quantify the growth kinetics of MCTs and compare the therapeutic effect of different inhibitors at different concentrations, a voxel-based volume measurement was utilized to provide volume growth information over 11 days. Fig. 3A showed the quantitative plots of spheroid growth in inhibitors 2-ME, AZD1208, and R-keto with the concentrations of 1, 10, and 25  $\mu M$  over 11 days. First, we found that all three inhibitors (2-ME, AZD1208, and R-keto) at the concentrations of 10 and 25  $\mu M$  significantly decreased spheroid volumes compared to the control group except for AZD1208 at day 6. Particularly, MCTs treated with 2-ME at concentration of 10 and 25  $\mu M$  showed extremely slow volume growth and even

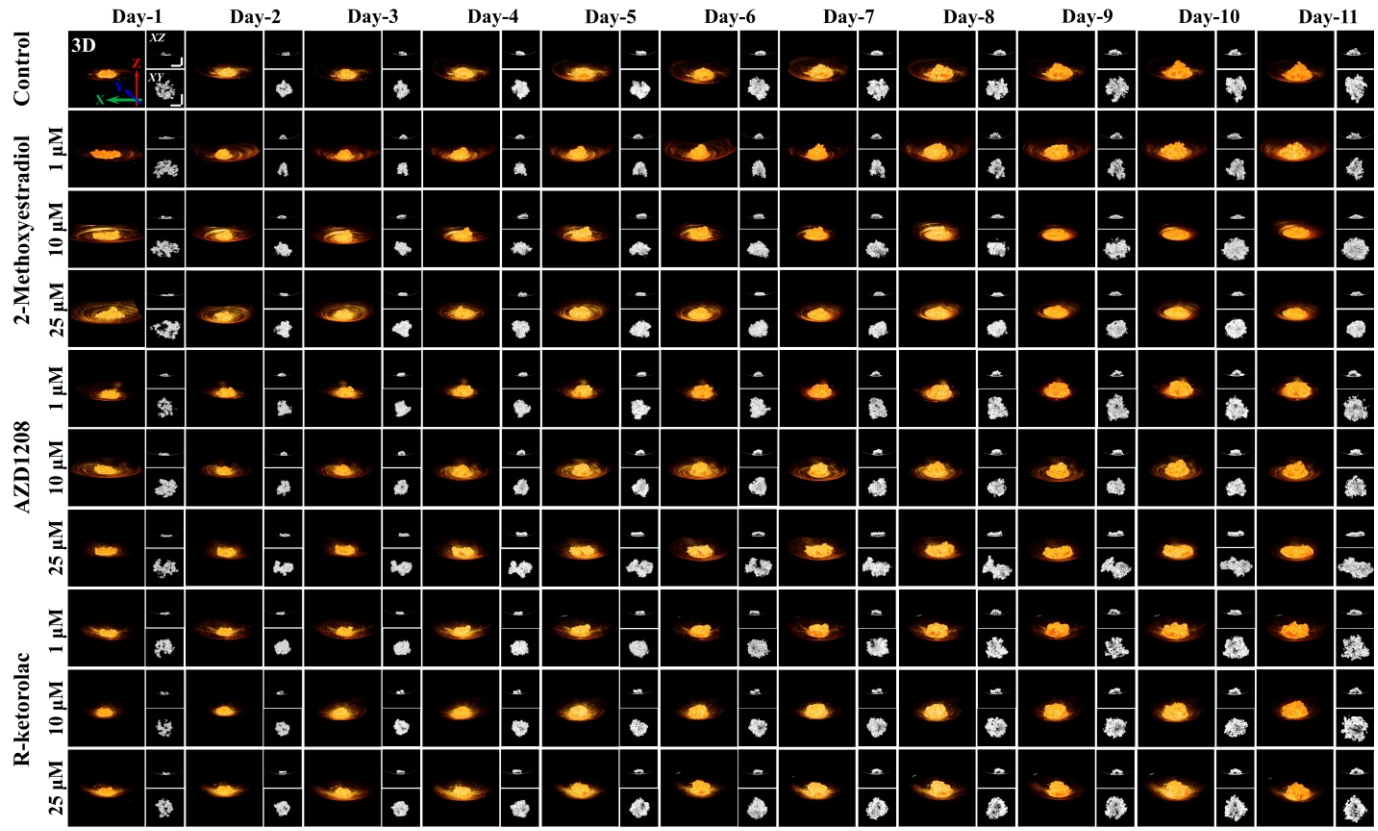


Fig. 2. Growth dynamics visualization of OVCAR4 tumor spheroids in inhibitors 2-Methoxyestradiol, AZD1208, and R-Ketorolac with concentrations of 1, 10, and 25 μM over 11 days. Each spheroid was displayed with a 3D (orange), XZ (top right), and XY (bottom right) dimensions. Scale bar is 500 μm.

started declining after day 9 (10  $\mu$ M) (Fig. 3A). The therapeutic effect on the volume growth of MCTs treated with 2-ME, AZD1208, and R-keto with concentrations of 10 or 25  $\mu$ M ranged from high to low, respectively (Fig. 3A). Second, only MCTs treated with 2-ME showed significant concentration-dependent manner, i.e., MCTs treated with 2-ME at concentrations of 25  $\mu$ M showed significant decrease compared to that of 10  $\mu$ M and even more than those treated with 1  $\mu$ M. Third, although the effect of the concentration of 1  $\mu$ M was not always significant, all three inhibitors still showed similar trend in the decrease of spheroid volumes compared to the control group (Fig. 3A). Fourth, when we looked at the statistical analyses among different inhibitors, at concentrations of 10 and

this limitation of H&E process highlighted the advantage of OCT for imaging the spheroid growth and monitoring the therapeutic effects of drugs.

#### B. Tumor spheroid tissue uniformity

OCT images provided information on the morphology and growth kinetics of MCTs. With further calculation of the dispersion degree of the intensity difference in specific areas, OCT structure images were able to reveal the distribution characterization of the tissue uniformity. The uniformity degree images showed the homogeneity and heterogeneity of the internal tissue within MCTs, which could not be directly observed from the intensity-based OCT images. Figure 4

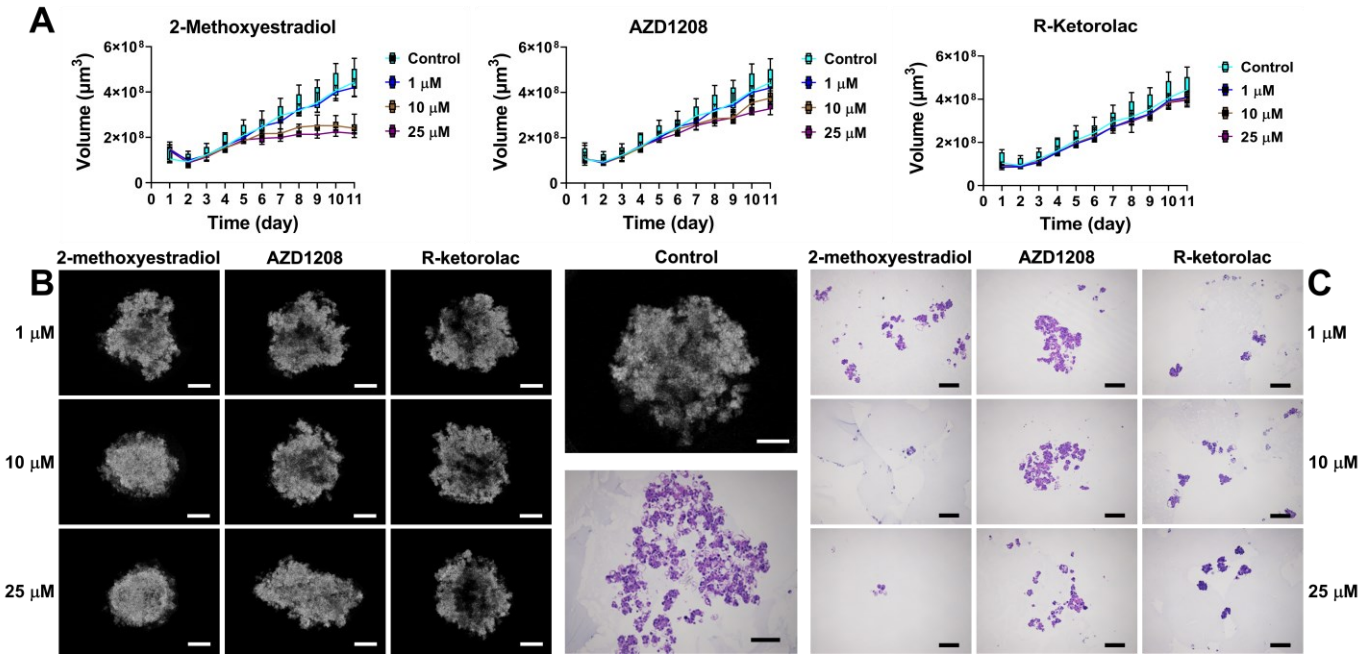


Fig. 3. Growth kinetics of tumor spheroids under the treatment of inhibitors with specific concentrations. A, plots of growth kinetics of OVCAR4 spheroids based on OCT. B, intensity-based OCT images of OVCAR4 tumor spheroids with inhibitor treatments. C, micrographs of H&E stained inhibitors treated OVCAR4 MCTs. On the 11th day, one set of the MCTs was used for histology preparation. Scale bar: 300 μm.

 $25~\mu M$ , MCTs treated with 2-ME had shown significant decreases in spheroid volumes compared to the other two inhibitors (AZD1208 and R-keto), while there is no significant difference between AZD1208 and R-keto.

Besides the volume change, OCT was also able to reveal the microstructure inside the MCTs in response to the inhibitors. In the enface OCT images of OVCAR4 MCTs with inhibitor treatments (Fig. 3B), we observed that the tumor spheroids treated with 2-ME at 10 and 25  $\mu M$  and AZD1208 at 25  $\mu M$ concentrations became smaller and denser compared to the control as well as other groups. MCTs treated by R-keto (1, 10, and 25  $\mu$ M), AZD1208 (1 and 10  $\mu$ M), and 2-ME (1  $\mu$ M) had shown more irregular shapes. The internal tissues showed a dispersed distribution that was filled with holes and empty areas within spheroids, which were similar to those observed in control group both under OCT and H&E staining (Fig. 3B and C). Unfortunately, due to the destructive nature of the H&E staining process, MCTs disintegration was observed in most of the H&E results, which made it difficult to perform a side-byside comparison with our OCT results. While on the other hand,

showed the distribution of tissue uniformity within MCTs and the effect of inhibitors on tissue uniformity. We observed that the tissue uniformity of MCTs presented an irregular and dispersed distribution in the control sample on day 5 (Fig. 4A). In the probability statistics of the uniformity degree in MCTs without inhibitors on day 5 (Fig. 4B), the uniformity degree showed a distribution of two peak values. We set the average value (40.55) of the uniformity degree corresponding to the two peak probabilities (39.2 and 41.9) as the threshold to separate the low and high uniformity degree tissues within MCTs. As shown in Fig. 4C after applying the threshold, we clearly observed the distribution characterization of the tissue with low (red) and high (green) uniformity degrees within MCTs. The subfigures Figure 4C<sub>1-4</sub> showed the extracted tissue with low and high uniformity degrees and the corresponding overlay images with the original OCT intensity image. We then calculated the uniformity degree of tumor spheroids treated by inhibitors with different concentrations and the distribution of the tissue uniformity was shown in Fig. 4D. Compared to the tumor spheroid without treatments (control group), MCTs

treated with 2-ME (1 µM), AZD1208 (1 and 10 µM), and Rketo (1, 10, and 25 μM) showed a center-gathered homogeneity while the tumor spheroid with inhibitors of 2-ME (10 and 25 μM) and AZD1208 (25 μM) displayed a high degree of heterogeneity. With the threshold of the uniformity degree set, we separated the tissue with low and high uniformity degrees within spheroids (Fig. 4E). We found that high uniformity degree tissues gathered in the center of spheroids after the treatment of 2-ME (1 µM), AZD1208 (1 and 10 µM), and Rketo (1, 10, and 25 μM), which was similar as the uniformity distribution of the control sample. However, the treatment of 2-ME (10 and 25 µM) and AZD1208 (25 µM) caused low and high uniformity tissues to become more dispersed and intercrossed. The result of the tissue uniformity was consistent with the OCT structure, which confirmed that 2-ME with 10 and 25 µM concentrations and AZD1208 with 25 µM

showed the volumetric distribution of different tissues within the MCTs. Compared to the AZD1208 and R-keto inhibitors, MCTs that were treated with 2-ME with 10 and 25 µM showed more tissues with low uniformity on day 11, as shown in Fig. 5A. Fig. 5B showed that the volume of tumor tissues with low uniformity increased between day 1 and day 8 and decreased from day 9 to day 11. Similar to the control group, all the three inhibitors did not cause the change in the volume growth of tumor tissues with low uniformity by day 11 compared to day 1. However, compared to the low uniformity tumor tissues, the volume of tumor tissues with high uniformity increased from day 1 to day 11. The volume of high uniformity tissues within MCTs that were treated with 2-ME and AZD1208 for all concentrations was significantly smaller than that of MCTs treated with R-keto inhibitors and the control group. When the concentrations of 2-ME and AZD1208 inhibitors were higher,

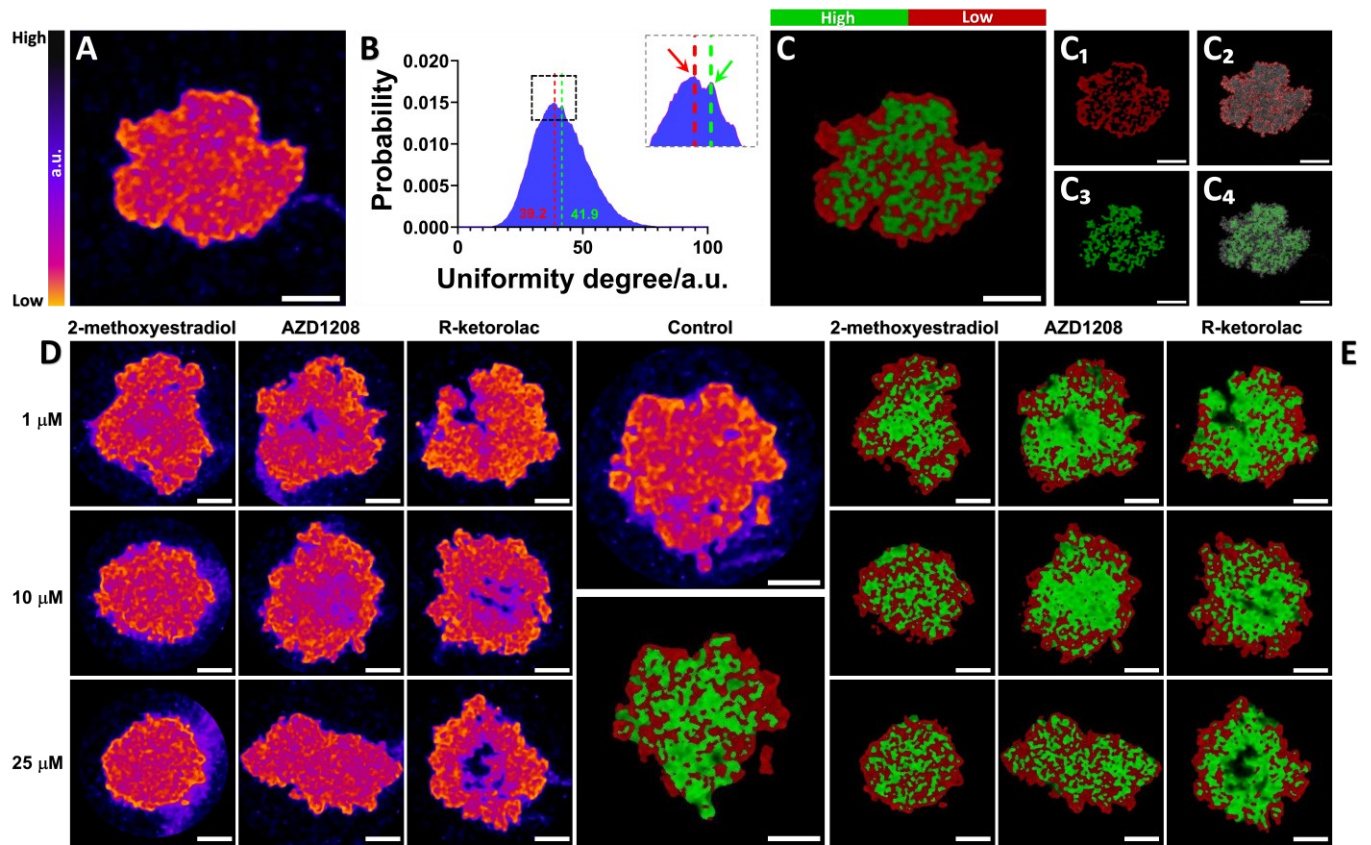


Fig. 4. Distribution characterization of the tissue uniformity degree within tumor spheroids treated with inhibitors with different concentrations. A, the distribution image of the uniformity degree in a tumor spheroid without inhibitor on day 5. B, the probability distribution of the uniformity degree of all tumor spheroids on day 5. C, the distribution of low and high uniformity degree tissues via the threshold of 40.55. C₁ and C₃, low and high uniformity degree tissues. C₂ and C₄, the overlay of low and high uniformity tissues with the OCT intensity image. D, the distribution image of the uniformity degree in tumor spheroids treated with inhibitors with different concentrations on day 11. E, the distribution of low and high uniformity degree tissues in tumor spheroids treated with inhibitors with different concentrations on day 11. Scale bar: 300 μm.

concentration not only restricted the volume growth and morphology but also affected the distribution of the tissue uniformity within MCTs.

We further calculated the volume of tissues with low and high uniformities within MCTs. Moreover, the ratio between the low and high uniformity tissue volumes was used to describe the relative change of the uniformity over time. Fig. 5 showed the 3D structure of low and high uniformity tissues within MCTs and the corresponding statistics. The 3D structure

the volume growth of high uniformity tissues became slower. The relative ratio between low and high uniformity tissues was around 50% before day 9 under the treatment of the three inhibitors and decreased after day 8 due to the decrease of low uniformity tissues and the increase of high uniformity tissues within MCTs.

C. Tumor Spheroid Intrinsic Optical Attenuation Contrast
The intensity-based OCT images was further utilized to

obtain the growth and distribution of necrotic tissues within MCTs based on the intrinsic optical attenuation coefficient. As shown in Fig. 6A, we monitored the volume growth of necrotic tissues within MCTs for different groups. We observed that the volumes of necrotic tissues under treatments of 2-ME at 10 and 25  $\mu$ M concentrations and AZD1208 with 25  $\mu$ M concentration

were smaller than that of other groups. Statistically, Fig. 6B showed that MCTs treated with 2-ME, AZD1208, and R-keto with 10 and 25  $\mu$ M concentrations had significantly smaller volumes of necrotic tissues compared to other groups. This tendency was consistent with the dynamic change of the volume of MCTs over 11 days. After we calculated the ratio between

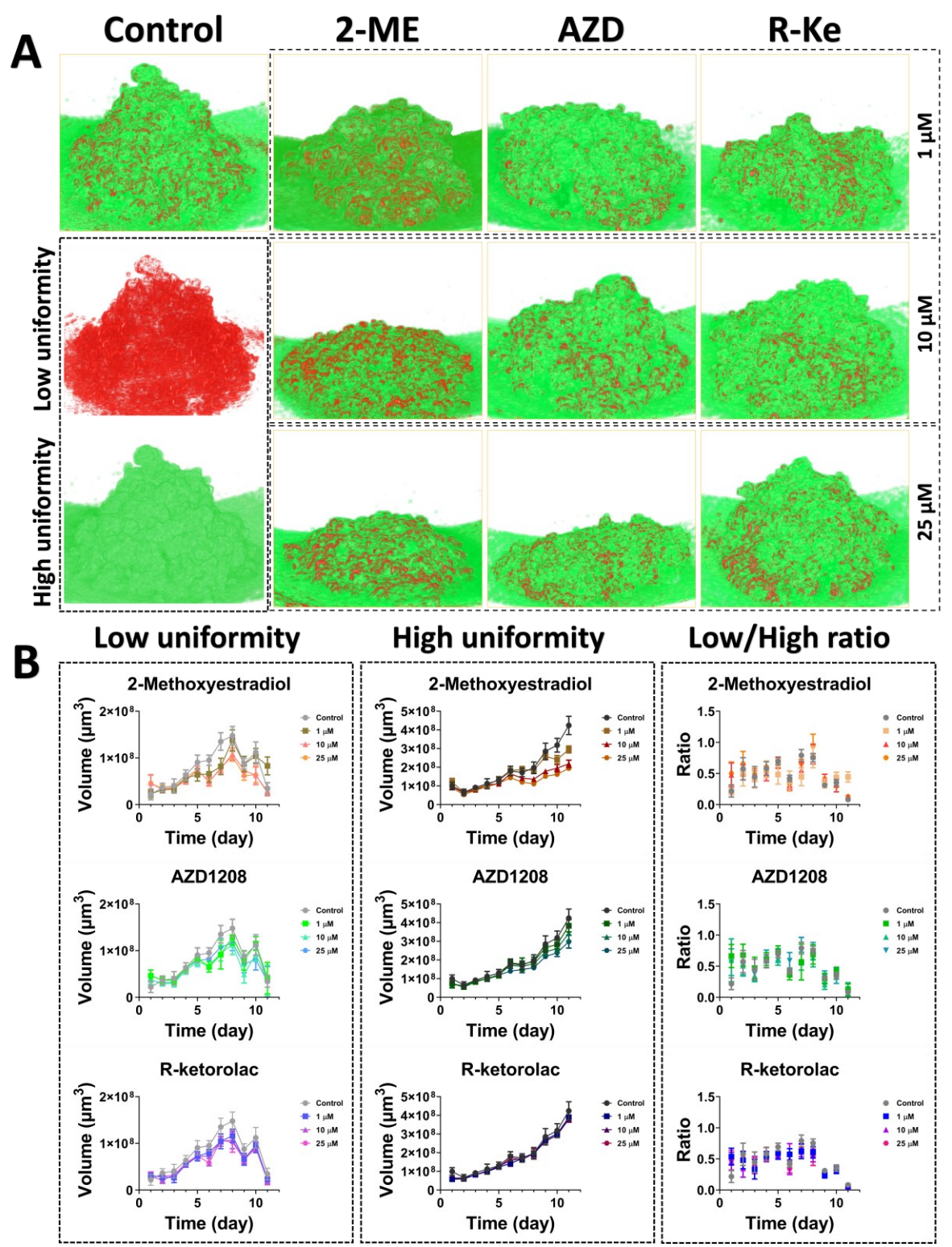


Fig. 5. 3D structure of tumor spheroid with low and high uniformities and the related statistics of dynamic changes of tumor spheroid volumes. A, 3D structures of tumor tissues with low and high uniformity within tumor spheroids on day 11. B, corresponding statistics of dynamic change of tumor tissue volumes over time. 2-ME, 2-Methoxyestradiol. AZD, AZD1208. R-Ke, R-Ketorolac.

necrotic tissues and whole MCTs, we found that the ratio kept increasing from day 1 to day 3 and maintained an equilibrium around 50% after day 3 for all the groups (Fig. 6C).

Fig. 6D showed the distribution of necrotic tissues within MCTs treated with the three inhibitors at different concentrations as imaged by OCT on day 11. We found that MCTs treated with 2-ME at 10 and 25  $\mu M$  concentrations showed tighter and more concentrated necrotic tissues than those of the control group and other treated MCTs. To verify the results of dead cell distributions that we calculated from OCT images, imaging by Operetta was carried out to detect the distribution of dead cells. Similar to OCT results, 2-ME at 10 and 25  $\mu M$  concentrations showed relatively compact dead cells within MCTs compared to the control and other groups (Fig.

#### IV. DISCUSSION

Effective treatment for recurrent epithelial ovarian cancer is a major, unmet public health need as the response rates of the patients are low with traditional chemotherapy. Drug Repurposing is an increasingly popular strategy in oncology due to the financial and logistical constraints of new drug development. An imaging tool that can rapidly screen and evaluate the repurposing of drugs based on the 3D tumor model is needed. Our results indicated that intensity-based OCT images effectively monitored the dynamic change of volume growth of MCTs under three inhibitors treatments of 2-MEl, AZD1208, and R-keto. With the different concentrations of inhibitors, OCT reliably revealed the difference in the volume growth of MCTs. In this study, we demonstrated that inhibitors

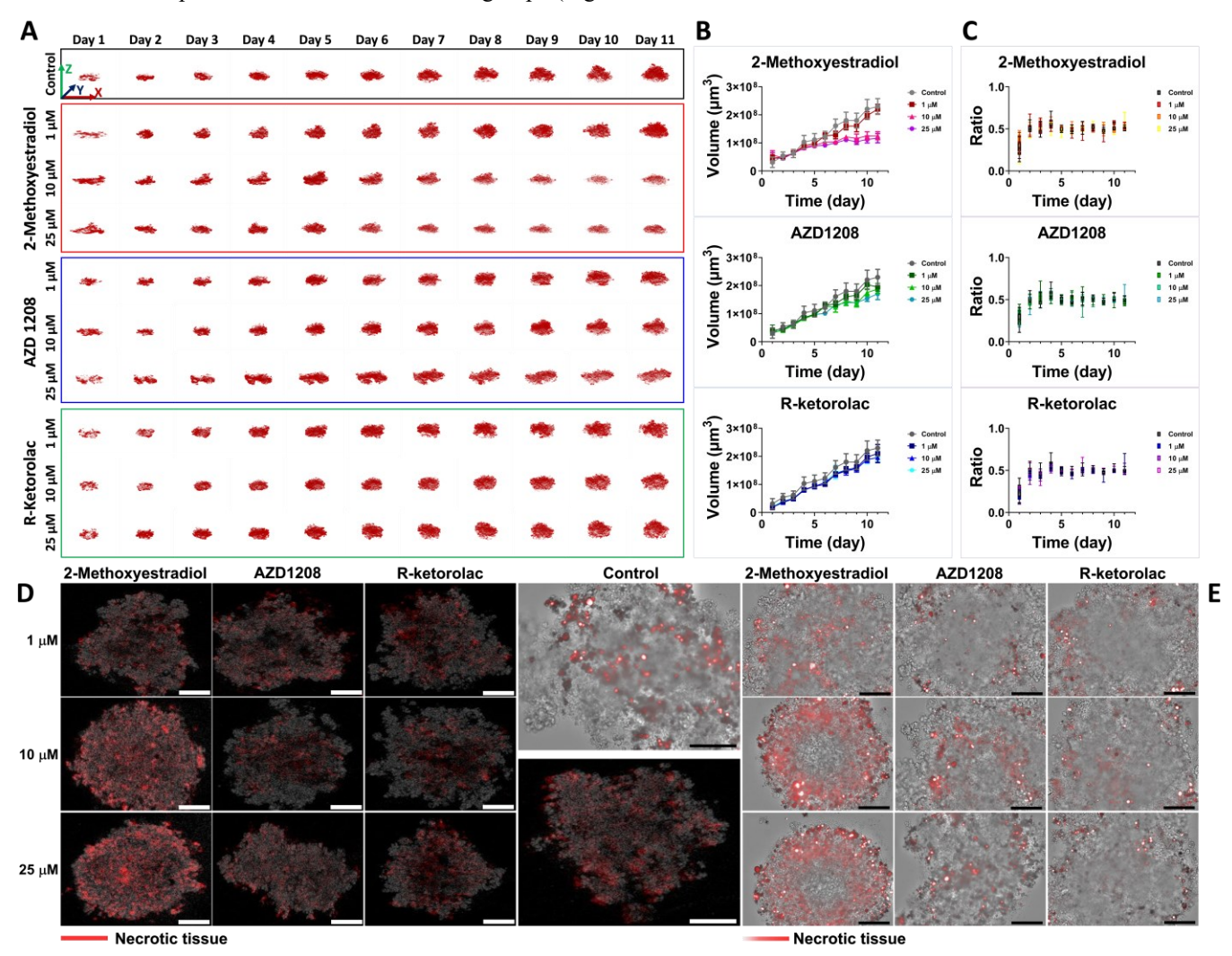


Fig. 6. 3D structure mapping and distribution of dead cells within MCTs by attenuation contrast and Operetta imaging. A, 3D structures of necrotic tissues within tumor spheroids under treatments of three inhibitors. B, dynamic change of the volume of necrotic tissues. C, the relative ratio between the volume of necrotic tissues and tumor spheroids. D, the distribution image of necrotic tissues in tumor spheroids treated with inhibitors with different concentrations from OCT on day 11. Necrotic tissues were marked by red and overlayed on OCT intensity images (gray). E, the distribution of necrotic tissues in tumor spheroids treated with inhibitors with different concentrations from Operetta on day 11. Red color indicated necrotic tissues. Scale bar: 300 μm.

6E). On the other hand, we cannot ignore the possible shedding of the dead cells from the spheroids as had been reported in other MCTs [17].

of 2-ME, AZD1208, and R-keto with concentrations of 10 and 25  $\mu$ M significantly inhibited the volume growth of MCTs. Therefore, 10 and 25  $\mu$ M 2-ME, AZD1208, and R-keto were effective in treating this specific high grade serous ovarian carcinoma subtype of tumors represented by OVCAR-4. This

result confirmed that OCT was capable of performing drug screening for more effective anti-cancer treatments. Previous reports stated that OCT was significantly more accurate when calculating the volume of MCTs compared to conventional diameter-based modalities [7, 8]. The volumetric shapes of MCTs in OVCAR-4 cell lines were extremely irregular as we can see from OCT 2D and 3D images (Fig. 3), thus our results were more accurate and reliable compared to traditional volume estimation methods. Although H&E staining of spheroids indicated the disintegration of spheroids with the drug treatments and loss of cells during the sample processing, the overall profiles of MCTs in response to different inhibitor treatments were consistent with the OCT intensity images. Moreover, this limitation of the H&E process highlighted the advantage of OCT for imaging the microstructure within the spheroids in a noninvasive and noncontact manner during growth (Fig. 4B).

The tissue distribution and properties of tumor spheroids were determined by cell growth, proliferation, and death which were directly affected by oxygen and nutrition. Particularly, heterogeneous glucose and ATP distributions and lactate accumulation within tumor spheroids influenced distribution of tumor cells to form various cell gatherings and tissue clusters [2, 18]. Drug therapies changed the microcirculation and nutrition distribution within tumor spheroids and were able to further induce the specific tissue distributions. These characterized tissue distributions were recorded via the backscattered signals of OCT and were able to be reconstructed by calculating the degree of uniformity of the OCT pixel intensity. Therefore, the intensity-based OCT images could also be further analyzed to reveal the uniformity of tumor tissues within MCTs. We separated the tissues with the low and high degrees of uniformity within MCTs and quantified the dynamic change of uniformity in volume growth over 11 days. Our results showed that the low uniformity tissue volumes initially increased, and then steadily decreased, whereas the high uniformity tissue volumes maintained the increased trend over 11 days. This phenomenon resulted in the ratio between low and high uniformity tissues within MCTs keeping a dynamic balance over 11 days. The relative ratio indicated that MCT tissues became more homogeneous with the growth of MCTs due to the majority of high uniformity tissues within tumor spheroids. Compared to the other treatment groups, higher concentrations of 2-ME and AZD1208 inhibitors induced less high uniformity tissues (Fig. 6B). This was also consistent with the volume change of MCTs (Fig. 4A). Moreover, less high uniformity tissues showed a more dispersed and intercrossed distribution in enface structures of MCTs, as shown in Fig. 4D and 4E. This indicated that the high concentration of 2-ME and AZD1208 inhibitors could affect the internal tissue distribution of MCTs.

The proliferation and growth of cells within MCTs could cause necrosis due to the absence of oxygen and nutrient transfer [19-22]. We observed that the volume change of necrotic zones within MCTs remained the same changing tendency with the dynamic change of MCTs volumes over time. The relative ratio between the volume of necrotic tissues and

MCTs kept approximately consistent in all groups (control and three inhibitors with 1, 10, and 25  $\mu M$  concentrations) over 11 days. This indicated that these three inhibitors only inhibited the volume growth over time but might not affect the relative size of necrotic tissues. The smaller volume and slower volume growth of necrotic tissues in 10 and 25  $\mu M$  of 2-ME and 25  $\mu M$  of AZD1208 treatment groups were caused by the inhibition of the volume growth of MCTs. However, it should be noted that the necrotic cells in spheroids often undergo dissolution and cast off from the spheroids [17]. Thus, the progressive increase in the dead cells populations that were cleared off from the tumor spheroids could also contribute to the decreased volume of MCT upon drug treatments.

The observation that the OCT analysis indicated the therapeutic potential of 2-ME and AZD1208 is highly significant. 2-ME, AZD1208, and R-keto, tested here, targeted three major pathways involved in ovarian cancer growth and progression, namely HIF1a [23, 24], Pim1/2 [25], and Rac1 [26, 27]. Although the anticancer effects of 2-ME were well characterized in breast cancer - primarily as an anti-estradiol compound [28], its potential and efficacy in inhibiting ovarian cancer growth were poorly understood. In a similar vein, while the amplification of Pim1 or Pim2 was seen in 15% of high grade serous ovarian carcinoma patients, the therapeutic potential of AZD1208 in ovarian cancer was yet to be defined. Likewise increased expression of Rac1 was observed in 11% of HGSOC patients [29, 30]. Our findings that 2-ME and AZD1208 inhibited the ovarian tumor volume by OCT identified them as potential candidates for targeted therapy in ovarian cancer. Although R-keto failed to inhibit tumor spheroid volume increase, the development of a hollow core could be seen upon the treatment of the spheroids with 10 µM and 25 µM of R-keto. Since similar hollowing has been attributed to either necrotic core induced cell death and loss or morphological changes [31], the effects of R-keto need further investigation.

#### V. CONCLUSION

In this study, we utilized OCT as a rapid screening tool to monitor the growth and microstructure change of MCTs under the therapeutics of 2-ME, AZD1208, and R-keto inhibitors over 11 days. The degree of uniformity and intrinsic optical attenuation contrast based on intensity-based OCT images were employed to characterize the uniformity distribution and necrotic tissue zones within MCTs. Our results demonstrated that 10 and 25 µM concentrations of 2-ME, AZD1208, and Rketo significantly inhibited the volume growth over time. The inhibitors of 2-ME, AZD1208, and R-keto did not induce effective necrosis within MCTs and there was a dynamic balance of the ratio between necrotic tissues and tumor spheroids. Furthermore, higher concentration of 2-ME and AZD1208 inhibitors caused the inhibition of volume growth of high uniformity tissues, but the ratio between low and high uniformity tissues kept consistent over time. In summary, these results confirmed that OCT was capable and could monitor the therapeutic efficacy of drugs using MCTs in, monitoring both at the from structural and tissue levels. Thus our results point to

the high clinical potential of using OCT and MCTs as a rapid platform for screening drug repurposing and anti-cancer drug.

#### REFERENCES

- [1] R. Siegel, J. Ma, Z. Zou, and A. Jemal, "Cancer statistics, 2014," *CA: a cancer journal for clinicians*, vol. 64, no. 1, pp. 9-29, 2014.
- [2] F. Hirschhaeuser, H. Menne, C. Dittfeld, J. West, W. Mueller-Klieser, and L. A. Kunz-Schughart, "Multicellular tumor spheroids: an underestimated tool is catching up again," *Journal of biotechnology*, vol. 148, no. 1, pp. 3-15, 2010.
- [3] D. V. LaBarbera, B. G. Reid, and B. H. Yoo, "The multicellular tumor spheroid model for high-throughput cancer drug discovery," *Expert opinion on drug discovery*, vol. 7, no. 9, pp. 819-830, 2012.
- [4] R. Venkatasubramanian, M. A. Henson, and N. S. Forbes, "Incorporating energy metabolism into a growth model of multicellular tumor spheroids," *Journal of theoretical biology*, vol. 242, no. 2, pp. 440-453, 2006.
- [5] X. Gong *et al.*, "Generation of multicellular tumor spheroids with microwell-based agarose scaffolds for drug testing," *PloS one*, vol. 10, no. 6, p. e0130348, 2015.
- [6] A. S. Nunes, A. S. Barros, E. C. Costa, A. F. Moreira, and I. J. Correia, "3D tumor spheroids as in vitro models to mimic in vivo human solid tumors resistance to therapeutic drugs," *Biotechnology and bioengineering*, vol. 116, no. 1, pp. 206-226, 2019.
- [7] Y. Huang *et al.*, "Optical coherence tomography detects necrotic regions and volumetrically quantifies multicellular tumor spheroids," *Cancer research*, vol. 77, no. 21, pp. 6011-6020, 2017.
- [8] F. Yan et al., "Characterization and quantification of necrotic tissues and morphology in multicellular ovarian cancer tumor spheroids using optical coherence tomography," Biomedical Optics Express, vol. 12, no. 6, pp. 3352-3371, 2021.
- [9] D. Huang et al., "Optical coherence tomography," science, vol. 254, no. 5035, pp. 1178-1181, 1991.
- [10] I. Abd El-Sadek et al., "Optical coherence tomography-based tissue dynamics imaging for longitudinal and drug response evaluation of tumor spheroids," Biomedical Optics Express, vol. 11, no. 11, pp. 6231-6248, 2020.
- [11] I. Abd El-Sadek *et al.*, "Three-dimensional dynamics optical coherence tomography for tumor spheroid evaluation," *Biomedical optics express*, vol. 12, no. 11, pp. 6844-6863, 2021.
- [12] D. A. Gil, D. A. Deming, and M. C. Skala, "Volumetric growth tracking of patient-derived cancer organoids using optical coherence tomography," *Biomedical Optics Express*, vol. 12, no. 7, pp. 3789-3805, 2021.
- [13] M. Sharma, Y. Verma, K. Rao, R. Nair, and P. Gupta, "Imaging growth dynamics of tumour spheroids using optical coherence tomography," *Biotechnology letters*, vol. 29, no. 2, pp. 273-278, 2007
- [14] Y. Guo et al., "R-Ketorolac Targets Cdc42 and Rac1 and Alters Ovarian Cancer Cell Behaviors Critical for Invasion and MetastasisR-Ketorolac Targets GTPases and Ovarian Cancer Cell Invasion," Molecular cancer therapeutics, vol. 14, no. 10, pp. 2215-2227, 2015.
- [15] C. M. Becker *et al.*, "2-Methoxyestradiol inhibits hypoxia-inducible factor-1α and suppresses growth of lesions in a mouse model of

- endometriosis," The American journal of pathology, vol. 172, no. 2, pp. 534-544, 2008.
- E. K. Keeton *et al.*, "AZD1208, a potent and selective pan-Pim kinase inhibitor, demonstrates efficacy in preclinical models of acute myeloid leukemia," *Blood, The Journal of the American Society of Hematology*, vol. 123, no. 6, pp. 905-913, 2014.
- [17] J. Debnath and J. S. Brugge, "Modelling glandular epithelial cancers in three-dimensional cultures," *Nature Reviews Cancer*, vol. 5, no. 9, pp. 675-688, 2005.

[16]

- [18] E. C. Costa, A. F. Moreira, D. de Melo-Diogo, V. M. Gaspar, M. P. Carvalho, and I. J. Correia, "3D tumor spheroids: an overview on the tools and techniques used for their analysis," *Biotechnology advances*, vol. 34, no. 8, pp. 1427-1441, 2016.
- [19] P. Kovacic and J. A. Osuna Jr, "Mechanisms of anti-cancer agents emphasis on oxidative stress and electron transfer," *Current pharmaceutical design*, vol. 6, no. 3, pp. 277-309, 2000.
- [20] T. J. Mitchison, "The proliferation rate paradox in antimitotic chemotherapy," *Molecular biology of the cell*, vol. 23, no. 1, pp. 1-6, 2012.
- [21] A. Baldock et al., "From patient-specific mathematical neurooncology to precision medicine," Frontiers in oncology, vol. 3, p. 62, 2013.
- [22] D. I. Wallace and X. Guo, "Properties of tumor spheroid growth exhibited by simple mathematical models," *Frontiers in oncology*, vol. 3, p. 51, 2013.
- [23] J. H. Ha et al., "LPA Induces Metabolic Reprogramming in Ovarian Cancer via a Pseudohypoxic ResponseMetabolic Programming by LPA," Cancer research, vol. 78, no. 8, pp. 1923-1934, 2018.
- [24] R. Radhakrishnan *et al.*, "Ovarian cancer cell-derived lysophosphatidic acid induces glycolytic shift and cancer-associated fibroblast-phenotype in normal and peritumoral fibroblasts," *Cancer letters*, vol. 442, pp. 464-474, 2019.
- [25] A. U. R. Aziz, S. Farid, K. Qin, H. Wang, and B. Liu, "PIM kinases and their relevance to the PI3K/AKT/mTOR pathway in the regulation of ovarian cancer," *Biomolecules*, vol. 8, no. 1, p. 7, 2018.
- [26] C. Wang, W. Wang, Y. Liu, M. Yong, Y. Yang, and H. Zhou, "Rac GTPase activating protein 1 promotes oncogenic progression of epithelial ovarian cancer," *Cancer Science*, vol. 109, no. 1, pp. 84-93, 2018.
- [27] L. G. Hudson, J. M. Gillette, H. Kang, M. R. Rivera, and A. Wandinger-Ness, "Ovarian tumor microenvironment signaling: convergence on the Rac1 GTPase," *Cancers*, vol. 10, no. 10, p. 358, 2018.
- [28] T. E. Sutherland et al., "2-methoxyestradiol is an estrogen receptor agonist that supports tumor growth in murine xenograft models of breast cancer," Clinical cancer research, vol. 11, no. 5, pp. 1722-1732, 2005
- [29] E. Cerami *et al.*, "The cBio cancer genomics portal: an open platform for exploring multidimensional cancer genomics data," *Cancer discovery*, vol. 2, no. 5, pp. 401-404, 2012.
- [30] J. Gao *et al.*, "Integrative analysis of complex cancer genomics and clinical profiles using the cBioPortal," *Science signaling*, vol. 6, no. 269, pp. pl1-pl1, 2013.
- [31] E. Steinberg *et al.*, "Rapid clearing for high resolution 3D imaging of ex vivo pancreatic cancer spheroids," *International journal of molecular sciences*, vol. 21, no. 20, p. 7703, 2020.